JOURNAL OF GEOPHYSICAL RESEARCH, VOL. 105, NO. D14, PAGES 17,983–17,993, JULY 27, 2000

Gravity waves in the tropical lower stratosphere: A model study of seasonal and interannual variability

M. Joan Alexander

Northwest Research Associates, Inc., Colorado Research Associates Division, Boulder, Colorado

Robert A. Vincent

Department of Physics and Mathematical Physics, University of Adelaide, Adelaide, Australia

Abstract. A model study is presented to clarify the relationship between gravity-wave properties observed in the stratosphere and the sources for the waves, presumed to be in the troposphere. The observations are balloon-borne radiosondes launched from Cocos Island in the tropical Indian Ocean (12°S, 97°E), and the analysis of these data is described in a companion paper [*Vincent and Alexander,* this issue]. The dominant time variations in the observed gravity wave activity are annual and quasi-biennial patterns in the zonal momentum flux and kinetic energy density. The background zonal winds at this site vary with the same periods, and these are known to be capable of causing dramatic variations in the observable properties of the waves even if the sources for the waves are constant in time. The results presented here clarify (1) the nature of the sources for the gravity waves observed in the stratosphere, (2) the limitations of the observations for observing the full range of gravity wave perturbations potentially present in the atmosphere, and (3) the role the observed waves can play in forcing the quasibiennial oscillation (QBO) in the zonal winds at this latitude. The stratospheric waves appear to originate near the height of the tropopause, so the source is apparently related to deep convection. No seasonal or interannual variations in the convection need be assumed to understand the observations. The waves at the tropopause appear to have a phase speed distribution that is narrowly confined near zero phase speed relative to the ground. The source is likely related to slowly propagating tropospheric convection and the wind near the tropopause. Variations observed in the stratospheric data are caused by both the wind shear in the stratosphere and the ability of waves with these characteristics to propagate vertically without severe dissipation. Higher phase speed waves may be present and could carry significant momentum flux vertically into the stratosphere and mesosphere but would be extremely difficult to see in these radiosonde data. The observed waves can contribute substantially to the descent of the eastward shear zones characteristic of the "westerly" phase of the QBO in the lower stratosphere zonal winds.

1. Introduction

The observations presented in the companion paper [*Vincent and Alexander*, this issue], (hereinafter referred to as VA) show large seasonal and interannual variations in gravity wave energy density and momentum flux in the stratosphere over the Cocos Islands. These are small, remote islands in the tropical Indian Ocean (12°S, 97°E) with no significant topography in the vicinity, lying about 1500 km southwest of Jakarta, Indonesia, and about 3500 km west of Darwin, Australia. The patterns in the time variations in the data suggest that convection may be an important source for these waves, because peaks in momentum flux and energy density occur during the wet seasons, December through May. With nearly six years of radiosonde data presented, the results also show an interannual variation that is apparently related to the quasi-biennial oscillation (QBO) in the zonal stratospheric winds.

Atmospheric models need details about the nature of gravity wave sources and the properties of the waves they generate in order to describe the basic zonal mean circulation and structure of the middle atmosphere. The existing body of observations suggests gravity waves can fill a broad spectrum of phase speeds, vertical and horizontal wavelengths, frequencies, and propagation

Paper number 2000JD900197.
0148-0227/00/2000JD900197$09.00

directions. These properties, as well as wave amplitudes, have been observed to vary in latitude, longitude, height, and time [e.g., *Hirota,* 1984; *Hamilton,* 1991; *Fritts and Nastrom,* 1992; *Eckermann et al.,* 1995; *Allen and Vincent,* 1995]. Such variations may greatly influence the seasonal, semiannual, and quasi-biennal wind oscillations in the middle atmosphere [*Saravanan,* 1990; *Ray et al.,* 1998; *Alexander and Holton,* 1997; *Dunkerton,* 1997; *Garcia and Sassi,* 1999].

The Cocos Island radiosonde observations reveal potentially important variations in the properties of gravity waves, but the observed patterns might also be too greatly affected by variations in the background winds to infer properties of the wave sources. *Alexander* [1998] compared a model of gravity waves propagating through observed background wind and stability profiles to several observation techniques that measure gravity wave temperature variance in the stratosphere. This work demonstrated how the inherent limitations of an observational technique can sometimes work in concert with the background wind variations to produce patterns similar to the observations, even though no variations in the sources of the waves were considered in the model. Observations in the lowermost stratosphere are best for inferring properties of gravity wave sources because they are close enough to the sources that the background wind shear will be less likely to influence the observations greatly. With these background wind effects in mind, we will use a model similar to that used by *Alexander* [1998] to aid in the interpretation of the radiosonde results described in the companion paper. In this study we aim to (1) test whether all of the observational results can be synthesized into a consistent physical model of a spectrum of vertically propagating gravity waves, (2) examine what that physical model can tell us about the nature and origins of the waves being observed, (3) compare the data and model details to critically assess what we can and cannot learn about the general properties of the full spectrum of waves that may be present in the tropical stratosphere from this effort.

The model study of gravity wave propagation and dissipation presented here will clarify the roles that source variations, wind filtering, wave refraction and Doppler shifting, observational limitations, and dissipation each play in forming the patterns seen in data. The model comparison will be shown to clarify the interpretation of these radiosonde data in terms of the properties of the waves generated by tropical convection and their role in driving the QBO.

2. Model Description

The model used here is the same as that applied by *Alexander* [1998], however, different gravity wave source spectra are input, and a range of different forcing altitudes in the troposphere are examined. This is a linear model describing one-dimensional gravity wave propagation through a vertically varying background atmosphere. The dispersion relation employed is

$$\hat{\omega}^2 = \frac{N^2k^2 + f^2(m^2 + \alpha^2)}{k^2 + m^2 + \alpha^2}, \quad (1)$$

where

$$\hat{\omega} = \omega - k\bar{u} \quad (2)$$

is the intrinsic frequency, k is the horizontal wavenumber, $\bar{u}$ is the background wind speed in the direction of propagation, ω is the ground-based frequency, N is the buoyancy frequency, m is the vertical wavenumber, f is the Coriolis parameter, $\alpha = (2H)^{-1}$, and H is the density scale height. This form of the dispersion relation (1) includes nonhydrostatic effects that are important at high frequencies, rotation effects that are important for low frequencies, and compressibility effects on waves with long vertical wavelengths ($O \sim 4\pi H$) [*Marks and Eckermann,* 1995]. At 12°S, $f = 3 \times 10^{-5}$ s^{-1}, and the inertial period is 2.4 days. This is the long-period limit for gravity waves at the Cocos Islands.

The gravity-wave source is specified as a spectrum of momentum flux versus phase speed in Figure 1. The spectrum is treated discretely and the waves are assumed to propagate linearly through a profile of background wind and stability. Each member of the spectrum in these calculations is assigned the same horizontal wavelength, but that wavelength is allowed to vary from case to case. The background fields are derived from the monthly-mean soundings of wind and temperature. Waves propagate vertically conserving action flux unless their amplitudes exceed the limit defined by the onset of convective instability. Then a "saturation" condition is imposed that cuts the amplitude to that limiting amplitude and considers the remainder of the action flux dissipated. Although a dynamic instability condition could be argued to be more appropriate in the lower stratosphere, recent research [*Lelong and Dunkerton,* 1998a, b] suggests that the choice of the convective versus dynamic instability condition will have little effect on the model results.

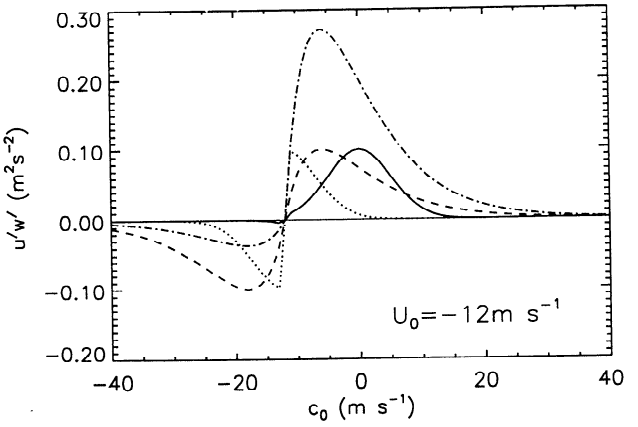

Figure 1. Examples of the four model source spectra described by equations (3) (solid line), (4) (dotted line), (5) (dashed line), and (6) (dotted-dashed line). The spectra describe the distribution of momentum flux amplitudes as a function of phase speed for the case of $\bar{u}_0$=12 m s^{-1}, c_w=6 m s^{-1}, and B_m=0.1 m^{2}s^{-2}.

In this one-dimensional model, the intrinsic frequency and vertical wavenumber vary with the background wind and stability, while the horizontal wavenumber remains constant. In the lower stratospheric region that we are studying, the buoyancy frequency N is approximately constant in both height and time, showing only weak vertical and seasonal variations, and the density scale height factor is also nearly constant, while the zonal wind changes considerably (see Figures 1 and 2 in the companion paper). So $\hat{\omega}$ and m are most directly related to changes in the background wind via (1), as is the intrinsic phase speed $\hat{c} = \hat{\omega}/k = c - \bar{u}$. The changes in $\hat{\omega}$ with $\bar{u}(z)$ are referred to as Doppler shifting, and the changes in m with $\bar{u}(z)$ are referred to as refraction.

To infer gravity wave properties from the balloon soundings, a parabolic fit to the profiles over the 18 to 25-km height range was first subtracted. The parabolic fit procedure will remove the mean profile and greatly reduce any gravity wave perturbations that have vertical wavelengths longer than ~ 7 km. Although use of this procedure carries the danger of distorting any long vertical wavelength waves ~ 7 km, the signal in these measurements of temperature and horizontal wind is very small at such long wavelengths and instead peaks near 2.5 km. Although longer vertical wavelength waves no doubt exist at this location [*McLandress et al.*, 2000], such waves are likely associated with much higher $\hat{\omega}$ and will be more prominent in measurements of vertical velocity [*Alexander et al.*, 2000] or those that exclude the shorter vertical wavelength waves [*McLandress et al.*, 2000]. The observations are also limited in their vertical resolution, so only waves with vertical wavelengths longer than 0.75 km can be observed. These effects will be referred to as observational filtering effects.

The model accounts for the observational effect by filtering the full, modeled spectrum in vertical wavelength, retaining only those waves in the 0.75 to 7-km range for the purpose of computing model energy densities and momentum fluxes before comparison to the data. Because the vertical wavenumber m changes with $\bar{u}(z)$, the observational filter can greatly affect what portion of the spectrum of waves is visible in the radiosonde data.

We will consider four types of gravity wave sources specified as spectra of momentum flux versus phase speed. An example of each of the four shapes is shown in Figure 1. The analytical forms of these spectra are

$$B_0(c) = \pm B_m \exp[-(c/c_w)^2 \ln 2], \tag{3}$$

$$B_0(c) = \pm B_m \exp\left[-\left(\frac{c-\bar{u}_0}{c_w}\right)^2 \ln 2\right], \tag{4}$$

$$B_0(c) = B_m \left(\frac{c-\bar{u}_0}{c_w}\right) \exp\left(1 - \left|\frac{c-\bar{u}_0}{c_w}\right|\right), \tag{5}$$

$$B_0(c) = B_m \left(\frac{c-\bar{u}_0}{c_w}\right) \exp\left(1 - \frac{\pm\bar{u}_0}{12\frac{\mathrm{m}}{\mathrm{s}}} - \left|\frac{c-\bar{u}_0}{c_w}\right|\right), \tag{6}$$

where c is the ground-based phase speed and $\bar{u}_0$ is the background wind at the source altitude z_0. The choice of $\pm$ depends on the sign of the intrinsic phase speed $\hat{c} = (c - \bar{u}_0)$ choosing the plus sign for $\hat{c} > 0$ and minus sign for $\hat{c} < 0$. The first two forms are Gaussian with half width at half maximum (HWHM) of c_w. Form (3) always peaks at $c = 0$. It will be anisotropic whenever $\bar{u}_0 \neq 0$. Form (4) is instead antisymmetric about $\hat{c} = (c - \bar{u}_0) = 0$, so it is an isotropic spectrum with equal amounts of eastward and westward momentum flux. The spectra given by (5) and (6) are both broader in phase speed for a given choice of c_w than the others. In these cases, c_w specifies the intrinsic phase speed where the spectrum peaks; this peak location remains constant for all values of $\bar{u}_0$, and c_w also affects the width of the spectrum. Form (5) is perfectly antisymmetric and isotropic, while (6) is anisotropic, emphasizing the flux carried by waves propagating upstream against the source level wind $\bar{u}_0$ relative to the downstream component. Form (6) is an approximation to the "transient mountain" forcing model for convectively generated gravity waves [*Pfister et al.*, 1993].

The coefficient B_m is specified in $\mathrm{m}^2\ \mathrm{s}^{-2}$ and represents the peak amplitude in the spectrum. These spectra describe the amplitudes of the pseudomomentum flux per unit density carried by each member of the spectrum. For the case of high-frequency waves this is simply the amplitude of the wave-mean covariance of horizontal and vertical wind $\overline{u'w'}$ commonly reported in observations. For low-frequency waves the pseudomomentum flux per unit density includes an extra factor $\overline{u'w'}(1 - f^2/\hat{\omega}^2)$. The choice of B_m will have an effect on the altitude where instability and dissipation occur for each wave. The total magnitude of the pseudomomentum flux (hereinafter referred to simply as the momentum flux) carried by the spectrum in each case (3)–(6) is given by a separate parameter F_{S0} related to B_0 via

$$F_{S0} = \varepsilon \sum_c (\bar{\rho}_0 |B_0(c)|) \tag{7}$$

where $\bar{\rho}_0$ is the background density at the source level. F_{S0} is the total momentum flux in the source spectrum. The factor ε is the intermittency of the wave forcing. It is specified here as a constant for all waves in the spectrum, but a choice of constant ε is made only for lack of any constraints on its dependence on wave properties. Constraints on the total flux crossing the tropopause do exist [*Alexander and Rosenlof*, 1996; *Dunkerton*, 1997; *Ray et al.*, 1998; *Alexander and Dunkerton*, 1999]. The flux carried by waves in the ± 30 m s^{-1} phase speed range at tropical latitudes is expected to be approximately $2 - 3 \times 10^{-3}$ Pa. We choose then to specify model parameters B_m, c_w, and

Table 1. Model Gravity Wave Parameters and the Values Considered

Parameter	Description	Values
B_0	source spectrum shape	equations (3), (4), (5), (6)
c_w	source spectrum width	(4,6,10,15,20) m s^{-1}
k	horizontal wavenumber	$2\pi/(300, 600, 1000, 1500, 2000)$ km
B_m	spectrum amplitude	(0.03, 0.10, 0.30) m^2s^{-2}
z_0	source altitude	(1.25, 8.75, 11.75, 14.75, 17.75) km

F_{S0}. Then letting ε be constant for all phase speeds, its value is determined by (7); ε will vary with numerical details of the specified spectrum, such as the number of waves in the spectrum or the phase speed resolution chosen. However, the physically important properties B_m and F_{S0}, which, respectively, determine the onset of instability and the magnitude of the mean-flow forcing associated with dissipating waves, are both observationally constrained and not sensitive to the arbitrary choice of spectral resolution. Note that the portion of the specified spectrum with $c \sim u_0$ will not, in general, be able to propagate vertically above the source level because the instability threshold for those waves occurs at very small amplitudes.

We focus here on the zonally propagating waves in the observations. These carry the majority of the momentum flux and may be important in driving the QBO in stratospheric winds. A discussion of the meridionally propagating waves appears in section 4.

There are five important free parameters in the model described in section 2: B_m, c_w, z_0, k, and the spectral shape (3)– (6). The sixth parameter F_{S0} behaves as a simple scaling factor for the problem, and it is reasonably well constrained, so it can be determined from a scaling analysis of the best fit later. The momentum fluxes determined from the observations are uncertain because of the unkown factor $\hat{\omega}$. The best fit model scaling factor for the flux may be thought of as another means of estimating $\hat{\omega}$ for the observations.

Because the model is a simple linear one, we can perform many calculations to explore the parameter space: 1500 model runs were completed, and the observationally filtered time series of momentum flux and energy density were computed for each. The parameter values considered in this study are listed in Table 1. The quality of the fit of the model will be judged from (1) the magnitudes of the linear coefficients of correlation between modeled and observed time series of zonal momentum flux and kinetic energy density and (2) the smallness of the intercepts of these linear correlations. A perfect correlation would have a coefficient of unity and an intercept of zero.

3. Results

The observations clearly show a dominance of eastward propagating waves and eastward momentum flux. A dominance of eastward propagating waves in observations of tropical gravity waves in the stratosphere has been reported elsewhere [*Hamilton and Vincent,* 1995; *Sato and Dunkerton,* 1997; *Tsuda et al.,* 1994; *Shimizu and Tsuda,* 1997]. Two hypotheses to explain this anisotropy in gravity wave activity have been proposed. (1) The waves are forced lower in the troposphere with an approximately isotropic spectrum, but the westward waves are preferentially filtered out as they propagate through the westward winds in the upper troposphere leaving the eastward waves to dominate the spectrum in the lower stratosphere. (2) The mechanisms for gravity wave generation preferentially excite waves in the upper troposphere that propagate eastward. We now test these two hypotheses with the model and observation comparisons.

3.1. Model Fit for a Low-Altitude, Isotropic Source

Hypothesis 1 above can be tested by inputting an isotropic gravity wave source to the model at low altitudes and allowing the tropospheric winds to filter the spectrum of waves before they reach the stratosphere. Figure 2 shows vertical profiles of the zonal winds for the two seasons (December-January-February and April-May-June) in which the observed gravity wave activ-

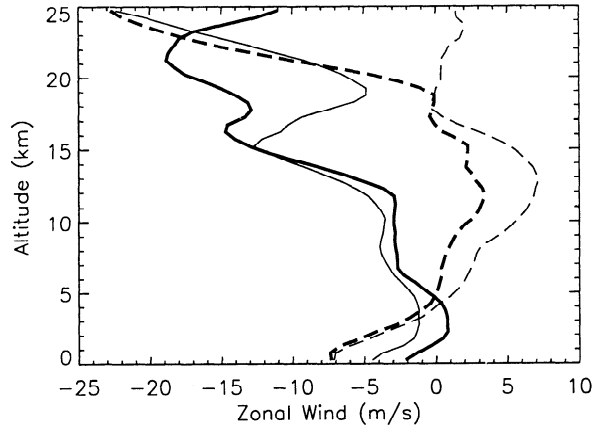

Figure 2. Background zonal winds for two seasons: (1) December-January-February (solid lines) when the gravity wave activity is at its peak and (2) April-May-June (dashed lines) when wave activity is a minimum. The thick lines include only years when the (quasi-biennial oscillation) is in the easterly phase, and the thin lines show only years with the QBO in the westerly phase.

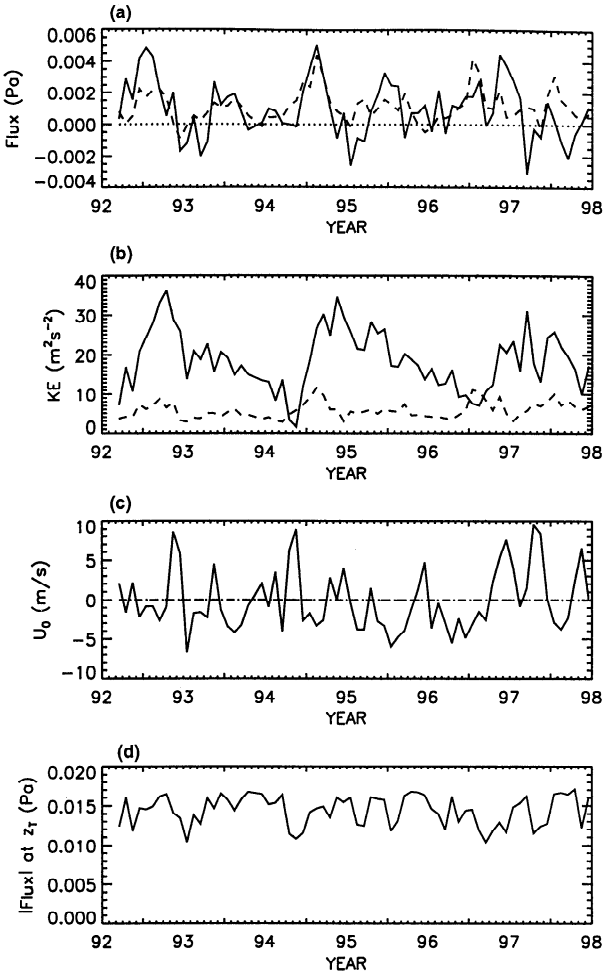

Figure 3. Time series showing results from a model fit (solid lines) assuming an isotropic source spectrum input lower in the troposphere. This is the best case found for $z_0 \leq 8.75$ km. The momentum flux time series (a) is similar to the observations scaled by a factor of 4 (dashed line). (b) Energy density time series for this model case is very dissimilar to that observed (dashed line). (c) Background zonal wind at z_0. (d) Total momentum flux crossing the tropopause ($z_T = 17.75$ km) for this case.

ity is at its maximum and minimum, respectively (VA). Profiles of the QBO easterly and westerly phases are also shown for each of these seasons.

Figure 3 shows the best fitting model comparison to the data for cases with an isotropic source specified in the troposphere. The observations are plotted with dashed lines and the model fit with solid lines. The parameters for this case are listed in Table 2 ("low z_0, isotropic"). The predominantly westward tropospheric winds (Figure 2) filter the wave spectrum, leaving predominantly eastward momentum flux in the stratosphere (Figure 3a) with time variations similar to those observed. The model/data correlation for the flux time series is fairly high (0.39), but the correlation between the modeled and the observed energy density time series (Figure 3b) is quite low (0.24), and the fit very unrealistic. So although the tropospheric wind filtering of a low-altitude, isotropic source of gravity waves is a plausible mechanism for explaining the momentum flux observations, the additional constraint provided by the energy density time series tells us that this scenario does not explain the radiosonde observations well at this site. The flux carried by vertically propagating waves into the stratosphere is plotted in Figure 3d. It varies $\sim \pm 25\%$ about the mean value 0.014 Pa. This value is larger than the constrained range of total gravity wave momentum flux at tropical latitudes discussed in section 2 but includes a wider range of phase speeds. Although the model specifies a purely constant flux input of 0.054 Pa (Table 2), some of the waves input near $c \sim u_0$ in the source spectrum are unstable and strongly damped, and others are filtered via dissipation between z_0 and the tropopause.

Results using the source spectrum (5) with a smaller c_w gave qualitatively similar results to those shown in Figure 3. Both lead to the same conclusion, that an isotropic spectrum input at low altitudes cannot fit both the momentum flux and the energy density time series derived from the observations.

3.2. Model Fit for a Tropopause "Transient Mountain" Model

Source shape (6) was designed to mimic the results of the "transient mountain" model for convective generation of gravity waves presented by *Pfister et al.* [1993]. In their model, the wave source is assumed to be a time-varying, localized adiabatic perturbation to the isentropic surface coinciding with the tropopause that also moves horizontally with speed U_T relative to the tropopause air parcels. The perturbation is assumed to grow exponentially to some maximum value then decay to zero with a time scale of ~5 hours that coincided with an observed convection event and coincident gravity wave observations in the stratosphere. As U_T increases in magnitude, the gravity wave spectrum becomes increasingly anisotropic with the flux in the upstream propagating waves exaggerated relative to the

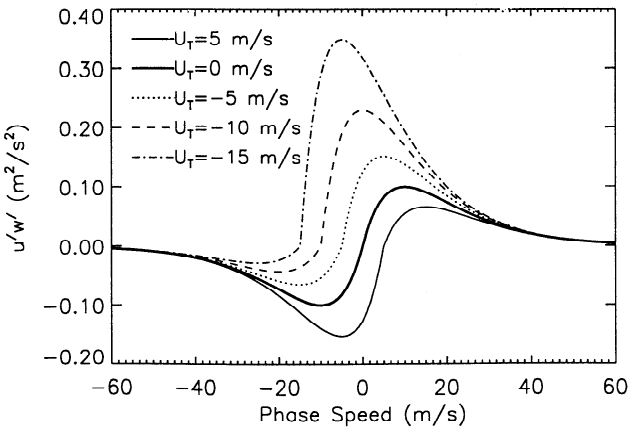

Figure 4. Source spectra for the "transient mountain" type of source spectrum, equation (6) with various values of $U_T = \bar{u}_0$. Compare to *Pfister et al.* [1993].

Table 2. Cases From Section 3 Used to Illustrate the Model Fit to the Observations†

Case	Best Fit Model	Low z_0 Isotropic	Transient Mountain Model
$B_0(c)$	equation (3)	equation (4)	equation (6)
c_w (m s^{-1})	6	15	10
$2\pi/k$ (km)	1500	1000	1000
B_m (m^{2}s^{-2})	0.3	0.3	0.1
F_{s0} (Pa)	0.014	0.054	0.034
z_0 (km)	17.75	8.75	17.75
Mean flux across the tropopause	0.0012 Pa	0.014 Pa	0.023 Pa
Flux correlations			
coefficient	0.57	0.39	0.61
intercept	0.4%	0.1%	7%
scale factor	8.0	4.0	1.4
KE correlations			
coefficient	0.66	0.24	0.17
intercept	2%	100%	300%

†The correlations between the modeled and observed energy density (KE correlations) and zonal momentum flux (flux correlations) are described in terms of the linear correlation coefficient and the intercept of the least squares linear fit (intercept) listed as the percent of the maximum value in the time series. High coefficients and low intercepts close to zero indicate good fits. A correlation coefficient > 0.3 indicates > 99.5% significance of the correlation relative to the null hypothesis but does not indicate a good fit unless the intercept is also small.

downstream component [see *Pfister et al.*, 1993, Figure 22].

The analytical approximation to this model in equation (6) becomes anistropic for nonzero winds in a manner similarly proportional to $U_T = \bar{u}_0$ Figure 4. The parameter c_w sets both the width of the spectrum and the intrinsic phase speed at which the spectrum peaks. An example fit using this type of source spectrum is listed as the "transient mountain." case in Table 2, and the results are shown in Figure 5. Excellent fits to the momentum flux time series were obtained with a source at the tropopause (Figure 5a), but the energy density time series was very poorly represented by this case (Figure 5b).

The degree of anisotropy in this source mechanism is tied to the tropopause wind speeds shown in Figure 5c. The dominance of westward winds at the source level then ensures that the source in equation (6) will generate primarily eastward propagating waves, similar to the observations. The source spectrum for this case will, however, always peak at the same intrinsic phase speed given by the parameter c_w. Associated with this constant peak intrinsic phase speed will be constant peak vertical wavelength and intrinsic frequency in time. These constants will tend to keep the stability characteristics of the source spectrum fairly constant in time, and there are therefore only weak time variations in the total magnitude of wave flux at the tropopause shown in Figure 5d. The "best fit" model case described in section 3.3 will illustrate how variations in the total flux propagating into the stratosphere are the key to explaining the observed energy density time series.

3.3. Best Fit Model Description, Tropopause Source, $c \sim 0$

The best fit example is shown in Figure 6. Figures 6a and 6b show the time series of zonal momentum flux and zonal kinetic energy density respectively in the stratosphere from both the radiosonde observations (dashed lines) and the best fit model (solid). This best fit was obtained for $c_w = 6$ m s^{-1}, $z_0 = 17.75$ km, $k = 2\pi/(1500$ km), and the spectral shape in equation (3). (See Table 2.) The input momentum flux in these plots was scaled to give a slope of unity in the energy density linear correlation. The value of F_{S0} input is then 0.014 Pa. The momentum flux time series for the observations in Figure 6a has been reduced by a factor of 8 from the scale on the left-hand side of Figure 10 in VA. This is well within the uncertainty for the magnitude of the observed flux because it depends on a parameterized value of $\hat{\omega}$ (VA). The best fit results suggest the mean value of $\hat{\omega}$ for the gravity waves in these observations is 8 times smaller or $\hat{\omega} = 2.1f$. This smaller intrinsic frequency is much closer to the frequency obtained from the hodograph analysis in VA. These model results suggest that these low-frequency waves with observable rotation in the horizontal wind hodograph dominate the total variances observed in the

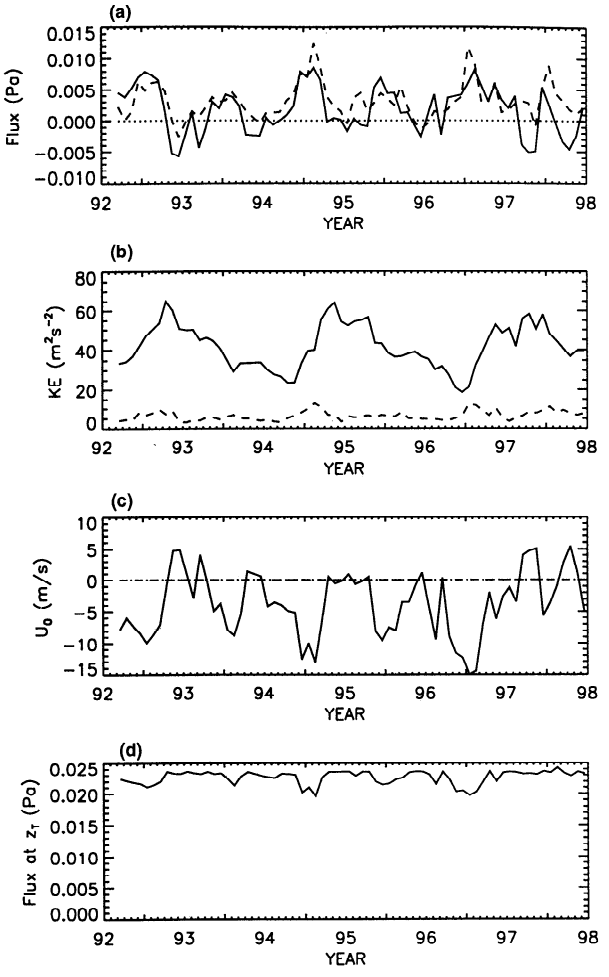

Figure 5. Time series showing results from a model fit (solid lines) using the "transient mountain" type source input at the tropopause. The momentum flux time series (a) is again similar to the observations, this time scaled by a factor of 1.4 (dashed line). (b) Energy density time series (as in Figure 3b), (c) the background wind at the source level z_0=17.75 km, and (d) total momentum flux crossing the tropopause for this case.

vertical profiles and that the hodograph analyses captured the average properties of the waves present in the observations well.

The value of F_{S0} of 0.014 Pa is about 5 times larger than existing constraints on the cross-tropopause flux. However, much of the flux input at the lower boundary is distributed in parts of the spectrum that either cannot propagate vertically as gravity waves ($\hat{\omega} < f$) or are unstable at the input amplitudes for the conditions present at the source level. Figure 7a shows the total magnitude of momentum flux being carried by the vertically propagating gravity wave spectrum at the tropopause (z_T = 17.75 km). The mean value over the entire record is only 1.2×10^{-3} Pa, and values range from 0.5 to 5.4×10^{-3} Pa, much smaller than the originally specified flux of 0.014 Pa. These values are still 1.3-6 times larger than observed Kelvin wave fluxes [*Andrews et al.*, 1987; *Sato and Dunkerton*, 1997].

It is apparent that the peaks in the cross-tropopause flux time series (Figure 7a) coincide with the peaks in both the observed energy and the momentum flux time series. These time variations in the net flux entering the stratosphere are key to understanding the time variations in the observed energy density. They arise naturally from the input source spectrum characteristics and the background atmosphere variations at the tropopause.

Figure 7b shows the time series of background wind at the source level z_0 = 17.75 km. Since the peak in the phase speed spectrum for this best fit case remains fixed at c = 0 m s^{-1} (equation (3)), the peak in intrinsic phase speed $\hat{c}$ and intrinsic frequency $\hat{\omega}$ input to the model vary considerably in time: $\hat{c}$ and $\hat{\omega}$ will be small when $\bar{u}_0$ is weak and will be larger when $\bar{u}_0$ is strong. Because the winds at z_0 are predominately westward, the wave momentum flux spectrum is dominated by eastward propagating waves in the best fit model because the spectrum always peaks at c = 0 m s^{-1}.

The best fit model suggests that the waves are forced high in the troposphere near the tropopause and that they have low phase speeds c. These are the two key constraints on the model fit. The results are less sensitive to the horizontal wavelength but constrain these to be, on average, $\sim$ 1000 km or longer. The sensitivity to the wave amplitudes at the source level (given by the parameter B_m) is similarly weak. Both k and B_m similarly control the degree of dissipation of the wave spectrum and control the ratio of the maxima to the minima in the modeled energy density time series.

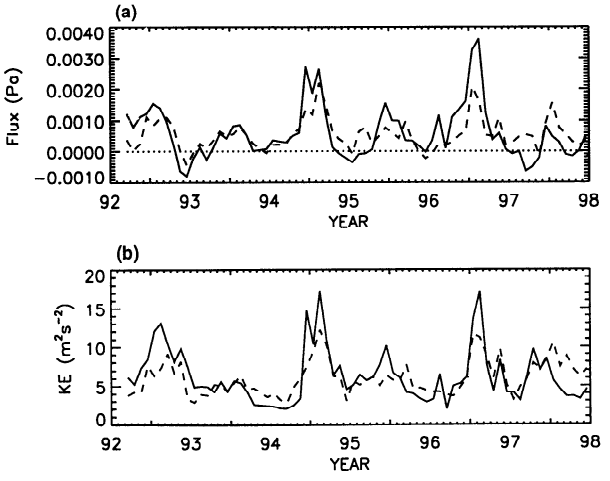

Figure 6. Time series of monthly mean (a) zonal momentum flux and (b) zonal kinetic energy density in the stratosphere averaged over the altitude range 18-25 km. The solid lines show the "best fit" model. The dashed line in (Figure 6a) is the flux inferred from the observations divided by a factor of 8.0. This factor suggests that the intrinsic frequencies of the waves observed are on average, lower than assumed, closer to $\sim 2f$ than $\sim 16f$.

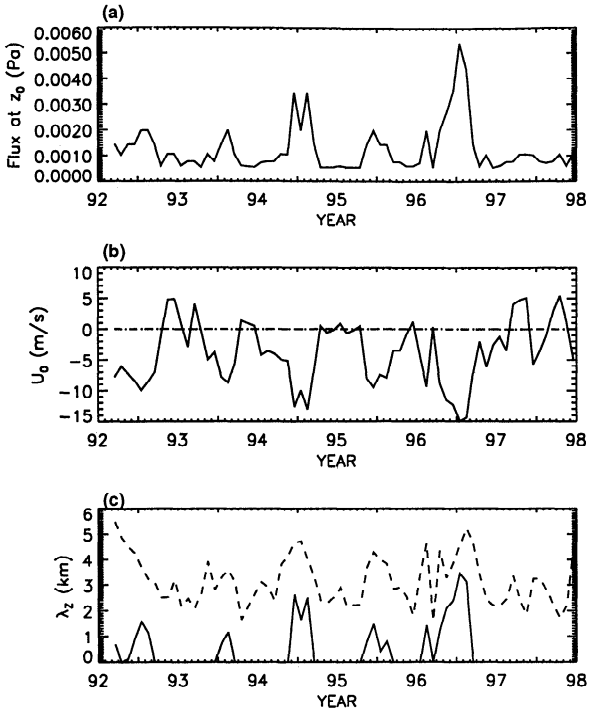

Figure 7. Time series showing results from the "best fit" model. (a) Total momentum flux carried vertically by waves across the tropopause. (b) Background zonal wind at the source level. (c) Vertical wavelength associated with the peak of the spectrum at the source level (solid line) and energy-weighted average vertical wavelength in the stratosphere 18-25 km (dashed line).

The changing cross-tropopause momentum flux is related to the changes in m and $\hat{c}$ in time. At 12°S the minimum gravity wave $\hat{c}$ is f/k=7 m s^{-1} for the best fit model ($\hat{c} = 7$ m s^{-1} approximately defines the inside of the dense ring of points plotted in VA Fig. 9). Therefore when $\bar{u}_0$ is small, most of the waves input to the model have $\hat{c} < 7$ m s^{-1} and $\hat{\omega} < f$, so most of the spectrum cannot propagate vertically, and the fluxes at that time are very small. The time series of vertical wavelength at the peak in the input spectrum is shown in Figure 7c (solid line). When the background zonal winds are strongest, waves with $c = 0$ have their largest vertical wavelengths. Waves with very short vertical wavelengths have $\hat{c} < 7$ m s^{-1} and $\hat{\omega} < f$. Also shown with the dashed line in Fig. 7c is the mean vertical wavelength (weighted by $\overline{u'^2}$) observable in the stratospheric zonal wind perturbations from the model. The average value is comparable to the vertical wavelengths in the observations.

The best fit model suggests that hypothesis 2 is more correct for the waves observed in these Cocos Island radiosonde data. In agreement with hypothesis 2, the "best fit" model suggests that the dominance of eastward flux in these observations arises from a gravity-wave source that preferentially generates waves with phase speeds close to zero relative to the ground, and it generates them at high altitudes where the winds are predominantly westward. The time variations in Figure 6 simply follow the variations in wave momentum flux shown in Figure 7a for this type of source.

3.4. QBO Forcing

The waves in the model suffer dissipation in the lower stratosphere as they propagate vertically through the background winds. Figure 8a shows the zonal force driven by gravity wave dissipation in the 18 to 25-km region in the best fit model case. The force X is computed from the vertical gradient in the wave momentum flux,

$$X = -\frac{\varepsilon}{\bar{\rho}} \frac{\partial}{\partial z} (\bar{\rho} \overline{u'w'}).$$

The shaded background in Figure 8a shows regions of westward background winds < -10 m s^{-1} to illustrate the QBO variations.

The total momentum flux carried by the waves in the model is a substantial fraction of the total estimated wave flux needed to drive the QBO [*Dunkerton*, 1997], but these fluxes are very irregular in time, and the fluxes are strongly anisotropic, favoring eastward flux. The result is that the mean-flow forcing is primarily important in driving the descent of the eastward shear of the QBO (called the "westerly phase"). Forcing in the westward shear zones (easterly phase) is comparatively small. Figure 8a represents the total zonal force, including all the waves in the model spectrum, but it should be noted that the importance to the QBO could be less than implied here if the waves at this site are not representative of the latitude band.

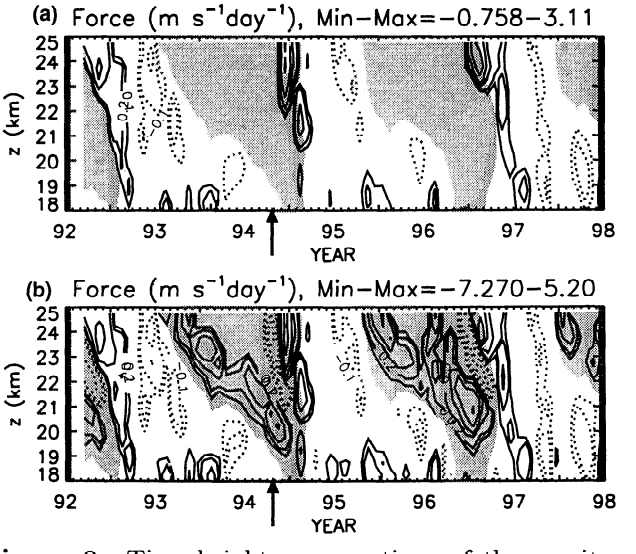

Figure 8. Time-height cross sections of the gravity-wave-driven force on the zonal winds (a) estimated from the "best fit" model, and (b) the erroneous estimate that would be derived using the same wave spectrum as in the model but filtered to include only those waves that could be observed in the radiosonde data. Arrows mark the Oct 1994 example described in the text.

Although it might be tempting to use the vertical variations in momentum flux observed directly to compute the mean flow forcing, we would next like to underscore the errors that would result from such an analysis. The radiosonde observations cannot see all the waves in the model spectrum at all heights. Instead, the vertical shear causes refraction of the waves, shifting them to different vertical wavelengths at different heights, and moving some of the wave activity in and out of the observable range of vertical wavelengths, 0.75-7.0 km. These effects were discussed by *Alexander* [1998]. When these limitations of the observations are taken into account so that the model momentum fluxes are filtered to include only the observable waves at each height, the momentum flux then appears to have a different vertical profile. If this vertical profile, including only the observable portion of the momentum flux were used to compute the zonal force on the background flow via (8), the result shown in Figure 8b would be obtained. The differences between 8a and 8b are dramatic, particularly in the westward phase (shaded regions) where large ficticious eastward gravity wave forcing would now be predicted.

In October 1994, for example, the stratospheric winds increase from near zero to -20 m s^{-1} (westward) then decrease again to -5 m s^{-1} by 25 km. This wind shear causes refraction of eastward propagating waves to vertical wavelength > 7 km above 19-km altitude. These waves are then refracted again to smaller vertical wavelength < 7 km above 22 km altitude. These waves suffer no dissipation, hence no force appears in Figure 8a at this time The fact that some of the waves are only visible in the radiosonde profiles at certain altitudes leads to a nonzero gradient in the "observationally filtered" flux and hence the force (8) is nonzero in Figure 8b at this same time. This example illustrates the danger in using observed momentum flux profiles to estimate mean-flow forcing. Severe errors could arise due to the natural limitations associated with the observation technique. Note that frequency analyses [e.g., *Fritts and Vincent,* 1987; *Sato et al.,* 1994] are not subject to the same problem because the wave frequency relative to the ground would not change across a shear layer.

4. Discussion

How well does the "best fit" model constrain the nature of gravity waves at this tropical site in the Indian Ocean? To address this question, we must first examine some of the assumptions inherent in the model design. In each model case, several parameters are assumed to be fixed in time. For the best fit model, the horizontal wavelengths of the waves and the source altitude are constant in time, and the ground-based phase speed distribution is also fixed in time. This spectrum has highly variable anisotropies in zonal wave momentum flux.

The unique qualities of the source spectrum in the "best fit" case (and those to which the model is most sensitive) are (1) the high altitude of the source and (2) the very low ground-based phase speeds in the spectrum which lead to the flux variations in Fig. 7a. One does not need to invoke time variations in the magnitude of the flux in the wave source spectrum because the background atmosphere variations give these naturally.

The fit constrains the ground-based phase speeds to be small (close to zero) but not too tightly. The peak in the spectrum could also be centered anywhere between ± 3 m s^{-1} without significant degredation in the model/data correlation. (This range is also somewhat subjective and could be broadened to ± 5 m s^{-1} with only moderate effect on the fit.) In the work of *Pfister et al.* [1993] the phase speed spectrum of the waves, generated with their transient mountain model, were dependent on the timescale τ over which the tropopause perturbations (the "mountain") grew and decayed and on the propagation speed of the convection. The timescale was set at $\tau = 5$ hours based on cloud-top height observations associated with the storm case that was examined in their work, and the storm moved slowly eastward at 1.5 m s^{-1}. In the limit that $\tau \to \infty$ and the storm speed $\to 0$, the model should reduce to a stationary mountain wave model. Thus if the timescale is long enough ($\tau \geq 5$ hours), and if the convection is approximately stationary relative to the ground, the transient mountain model would reproduce the wave source spectrum inferred from the best fit model, except that the wave amplitudes need not vary with the strength of the tropopause winds as they did in *Pfister et al.* [1993] model. Perhaps the fact, that the convective perturbations at the tropopause do not pose the rigid obstacle to the wind that a mountain does, means that at high wind speeds the obstacle in this case deforms in such a way as to reduce the flux predicted by the mountain wave analogy.

The convection need only be approximately stationary to give good agreement between model and observations. The Madden-Julian Oscillation (MJO) is an important modulation of tropospheric convection in the tropical Indian Ocean. The envelope of convection in the MJO propagates eastward at ~ 5 m s^{-1} [*Dunkerton and Crum,* 1995]. Tropical cyclones are also observed to propagate at slow speeds < 3 m s^{-1} in this region [*e.g. Pfister et al.,* 1993; *May,* 1996]. These may be the source of slow-moving tropopause perturbations that generate the low phase speed waves observed in these radiosonde data via a mechanism like the "transient mountain."

The model fit does not tightly constrain the horizontal wavelengths of the waves because the model is less sensitive to this parameter than to others. Still, long wavelengths $O \sim 1000$ km or greater are implied by the model/data correlation in section 3.3. In reality, these wavelengths are likely distributed in a broad spectrum rather than filling only a single wavelength peak. Therefore we must not regard the horizontal wavelength result too quantitatively.

Does the "best fit" with a narrow phase speed distribution confined tightly near zero imply that higher phase speed waves are absent? The answer is no, and in fact, these waves are likely to be present in the tropical stratosphere [*Alexander and Pfister,* 1995; *McLandress et al.,* 2000], but their time-integrated amplitudes of momentum flux must be small relative to the low phase speed waves. As a test, the "best fit" model was modified by adding a low-amplitude background flux at all phase speeds. With this background flux set at $\leq$5% of the peak value at zero phase speed, the fit to the observations was not seriously affected. However, with the background flux set to 10% or larger of the peak, the additional high phase speed flux began to degrade the correlation. Considering a total phase speed range of ± 60 m s^{-1}, the 5% background level increase would represent 48% of the total flux crossing the tropopause in the new spectrum leaving only 52% to the flux in the low phase speed waves between ± 10 m s^{-1}. So these high phase speed waves may be present in the lower stratosphere, and the fluxes they carry may be quite important to the upper stratosphere and mesosphere momentum budgets. Waves with phase speeds in the range $|c| \sim 10$ to 30 m s^{-1} may also be important to the QBO forcing in the lower stratosphere.

The time series of the meridional component of the momentum flux (see Figure 10 in VA) shows an annual variation with very little interannual variability. When the parameters from the best fit model were applied to the meridionally propagating waves, this time series was not well reproduced. Instead, the meridional waves require some seasonal variation in the model forcing with peaks during the February-March-April season and minima during August-September-March, in phase with the occurrence of deep convection (Fig.5 VA). With this seasonal cycle in forcing and an isotropic spectrum of waves input at 10.75 km, the meridional momentum flux time series can be approximated with a data/model correlation of $\sim$ 0.5. Because the meridional winds are very weak relative to zonal, the transient mountain mechanism may not generate these waves. They may instead be forced by the latent heating in deep convection. Cloud-resolving models of deep convection with weak shear in the upper troposphere [*Alexander and Holton,* 1997; *Piani et al.,* 2000] generate gravity waves with roughly isotropic phase speed distributions via this mechanism. However, low-frequency meridional gravity waves propagating from $\sim$ 10 km to the stratosphere may travel 10° of latitude or more before appearing over Cocos Island. Our one-dimensional (1-D) model assumes the background atmosphere is horizontally homogeneous, a potentially poor assumption in the meridional direction. A 3-D ray-tracing model may instead be required to study the meridionally propagating component of the wave spectrum in more detail. Note that the background zonal winds at the latitude of Cocos Island are fairly zonally symmetric so that propagation over large horizontal distances for the zonally propagating waves is not likely to seriously violate the model assumptions.

5. Summary

A linear model of gravity wave propagation was employed to clarify the interpretation of analysis results of radiosonde observations at Cocos Island. The observations show large oscillations in gravity wave activity on both seasonal and interannual timescales. The model study considered a broad range of gravity wave sources and possible characteristics of waves generated. The observed properties of the monthly-mean background winds and static stability were included as input to the model. The background winds, in particular, greatly affect the propagation properties of the waves and contribute to the seasonal and interannual variations in gravity wave activity observed in the stratosphere.

The model results suggest that the zonally propagating waves observed in the radiosonde data are forced at high altitude near the tropopause and have consistently very small zonal phase speeds less than 10 m s^{-1} and long horizontal wavelengths $\sim$1500 km. The source for these waves need not vary on seasonal or interannual timescales. Instead, the variations in the background wind preferentially allow propagation of larger or smaller amounts of wave activity into the stratosphere if the properties of the waves generated are as described above. This is not an effect of critical-level filtering of waves by the mean flow but more a result of time variations in the stability of waves with low ground-based phase speeds and long horizontal wavelengths near the tropopause.

The wave source is probably large-scale, slow-moving convection that causes perturbations at high altitudes near the tropopause. Higher phase speed waves could still be present in the stratosphere at this site but have amplitudes too small or vertical wavelengths too large to be observed. Their absence in the data do not imply any lack of importance of high phase speed waves to the middle-atmosphere momentum budget.

The waves observed have low intrinsic frequencies, $\sim 2f$ on average, and they seem to be well characterized by the separate hodograph analysis of the observations reported in the companion paper.

These waves probably contribute significantly to the descent of eastward shear zones in the eastward phase of the QBO (up to $\sim$50% if the waves at this site are representative of the latitude band) but punctuated in time. These waves will contribute relatively little to the QBO westward phase because most of the momentum flux they carry is eastward. Westward propagating waves important in the QBO westward phase may still exist but cannot be easily seen in these radiosonde observations.

Acknowledgments. Helpful comments by S.D. Eckermann, K. Sato, and two anonymous reviewers are gratefully acknowledged. This research was supported by the

National Science Foundation (NSF) Physical Meteorology grant ATM-989629, NSF POWRE program grant 9870502, and the Australian Research Council.

References

Alexander, M.J., Interpretations of observed climatological patterns in stratospheric gravity wave variance, *J. Geophys. Res., 103*, 8627-8640, 1998.

Alexander, M.J., and T.J. Dunkerton, A spectral parameterization of mean-flow forcing due to breaking gravity waves, *J. Atmos. Sci., 56*, 4167-4182, 1999.

Alexander, M.J., and J.R. Holton, A model study of zonal forcing in the equatorial stratosphere by convectively induced gravity waves, *J. Atmos. Sci., 54*, 408-419, 1997.

Alexander, M.J., and L. Pfister, Gravity wave momentum flux in the lower stratosphere over convection, *Geophys. Res. Lett., 22*, 2029-2032, 1995.

Alexander, M.J., and K.H. Rosenlof, Nonstationary gravity wave forcing of the stratospheric zonal mean wind, *J. Geophys. Res., 101*, 23,465-23,474, 1996.

Allen, S.J., and R.A. Vincent, Gravity wave activity in the lower atmosphere: Seasonal and latitudinal variations, *J. Geophys. Res., 100*, 1327-1350, 1995.

Andrews, D.G., J.R. Holton, and C.B. Leovy, *Middle Atmosphere Dynamics*, 489 pp., Academic, San Diego, Calif., 1987.

Dunkerton, T.J., The role of gravity waves in the quasi-biennial oscillation, *J. Geophys. Res., 102*, 26,053-26,076, 1997.

Dunkerton, T.J., and F.X. Crum, Eastward propagating 2-15 day equatorial convection and its relation to the tropical intraseasonal oscillation, *J. Geophys. Res., 100*, 25,781-25,790, 1995.

Eckermann, S.D., I. Hirota, and W.K. Hocking, Gravity wave and equatorial wave morphology of the stratosphere derived from long-term rocket soundings, *Q. J. R. Meteorol. Soc., 121*, 149-186, 1995.

Fritts, D. C., and G. D. Nastrom, Sources of mesoscale variability of gravity waves, II: Frontal, convective, and jet stream excitation, *J. Atmos. Sci., 49*, 111-127, 1992.

Fritts, D.C., and R.A. Vincent, Mesospheric momentum flux studies at Adelaide, Australia: Observations and a gravity wave-tidal interaction model, *J. Atmos. Sci., 44*, 605-619, 1987.

Garcia, R.R., and F. Sassi, Modulation of the Mesospheric Semiannual Oscillation by the Quasibiennial Oscillation, *Earth Planets Space, 51*, 563-569, 1999.

Hamilton, K., Climatological statistics of stratospheric inertia-gravity waves deduced from historical rocketsonde wind and temperature data, *J. Geophys. Res., 96*, 20,831-20,839, 1991.

Hamilton, K., and R.A. Vincent, High-resolution radiosonde data offer new prospects for research, *Eos Trans.AGU, 76(49)*, 497, 1995.

Hirota, I., Climatology of gravity waves in the middle atmosphere, *J. Atmos. Terr. Phys., 46*, 767-773, 1984.

Lelong, M.-P., and T.J. Dunkerton, Inertia-gravity wave breaking in three dimensions, 1, Convectively stable waves, *J. Atmos. Sci., 55*, 2473-2488, 1998a.

Lelong, M.-P., and T.J. Dunkerton, Inertia-gravity wave breaking in three dimensions, 2, Convectively unstable waves, *J. Atmos. Sci., 55*, 2489-2501, 1998b.

Marks, C.J., and S.D. Eckermann, A three-dimensional nonhydrostatic ray-tracing model for gravity waves: Formulation and preliminary results for the middle atmosphere, *J. Atmos. Sci., 52*, 1959-1984, 1995.

May, P.T., The organization of convection in the rainbands of tropical cyclone Laurence, *Mon. Weather Rev., 124*, 807-815, 1996.

McLandress, C., M.J. Alexander, and D.L. Wu, Microwave Limb Sounder observations of gravity waves in the stratosphere: A climatology and interpretation, *J. Geophys. Res., 105*, 11,947-11,967, 2000.

Pfister, L., K.R. Chan, T.P. Bui, S. Bowen, M. Legg, B. Gary, K. Kelly, M. Proffitt, and W. Starr, Gravity waves generated by a tropical cyclone during the STEP tropical feild program: A case study, *J. Geophys. Res., 98*, 8611-8638, 1993.

Piani, C., D. Durran, M.J. Alexander, and J.R. Holton, A numerical study of three dimensional gravity waves triggered by deep tropical convection, *J. Atmos. Sci.*, in press, 2000.

Ray, E.A., M.J. Alexander, and J.R. Holton, An analysis of the structure and forcing of the equatorial semiannual oscillation in zonal wind, *J. Geophys. Res., 103*, 1759-1774, 1998.

Saravanan, R., A multiwave model of the quasi-biennial oscillation, *J. Atmos. Sci., 47*, 2465-2474, 1990.

Sato, K., and T.J. Dunkerton, Estimates of momentum flux associated with equatorial Kelvin and gravity waves, *J. Geophys. Res., 102*, 26,247-26,261, 1997.

Sato, K., F. Hasegawa, and I. Hirota, Short-period disturbances in the equatorial lower stratosphere, *J. Meteorol Soc. Jpn., 72*, 859-872, 1994.

Shimizu, A., and T. Tsuda, Characteristics of Kelvin waves and gravity waves observed with radiosondes over Indonesia, *J. Geophys. Res., 102*, 26,159-26,171, 1997.

Tsuda, T., Y. Murayama, H. Wiryosumarto, S.W.B. Harijono, and S. Kato, Radiosonde observations of equatorial atmosphere dynamics over Indonesia, 2, Characteristics of gravity waves, *J. Geophys. Res., 99*, 10,507-10,516, 1994.

Vincent, R.A., and M.J. Alexander, Gravity waves in the tropical lower stratosphere: An observational study of seasonal and interannual variability, *J. Geophys. Res.*, this issue.

M. J. Alexander, Colorado Research Associates, 3380 Mitchell Lane, Boulder, CO 80301. (alexand@co-ra.com)

R. A. Vincent, Deptartment of Physics and Mathenatical Physics, University of Adelaide, Adelaide 5005, Australia. (robert.vincent@adelaide.edu.au)

(Received September 3, 1999; revised March 10, 2000; accepted March 14, 2000.)